Robotica (2017) volume 35, pp. 787–808. © Cambridge University Press 2015
doi:10.1017/S026357471500082X

Modular-robotic structures for scalable collective actuation

Jakub Lengiewicz*, Michał Kursa and Paweł Hołobut

Institute of Fundamental Technological Research of the Polish Academy of Sciences, Pawińskiego 5B, 02-106 Warsaw, Poland
E-mails: mkursa@ippt.pan.pl, pholob@ippt.pan.pl

(Accepted September 21, 2015. First published online: October 30, 2015)

SUMMARY
We propose a new class of modular-robotic structures, intended to produce forces which scale with the number of modules. We adopt the concept of a spherical catom and extend it by a new connection type which is relatively strong but static. We examine analytically and numerically the mechanical properties of two collective-actuator designs. The simulations are based on the discrete element method (DEM), with friction and elastic deformations taken into account. One of the actuators is shown to generate forces proportional to its volume. This property seems necessary for building modular structures of useful strength and dimensions.

KEYWORDS: Modular robots; Self-reconfiguration; Programmable matter; Actuators; Mechanical strength.

1. Introduction

One of the potential benefits of self-reconfigurable modular robots is their versatility. Such robots can dynamically adjust their physical configuration, which makes them superior to fixed-morphology robots in complex or unpredictable situations. The functionality of individual modules is usually very limited, and it is through collective work of many modules that the system obtains its desired capabilities, e.g., to change shape, lift objects or move.[1,2] The number of modules can potentially be increased and their size reduced. Extremely fine modular-robotic structures can be even seen as a realization of the programmable matter concept.[3]

The research on large-ensemble modular robots is still at an early stage. This is because of the high difficulty of the problem. Setting thousands or even millions of densely-packed microrobots to do collective work is far more complex than miniaturization and increasing the number of modules. A strong interplay exists between module design, reconfiguration control, power supply and communication. The present work partially concerns the first two problems.

Many module designs have been proposed as constituents of three-dimensional robotic systems. The *3D units*[4,5] form a cubic lattice and reconfigure by rotating and transporting their neighbors to adjacent locations. The *crystalline atoms*[6] are also based on a cubic grid, but reconfigure by extending into adjacent grid positions. These two designs have moving parts and special attachment mechanisms, which might be difficult to miniaturize. The *M-Blocks*[7] have a magnetic attachment mechanism, without moving parts, and reconfigure by rotating about their edges. However, their cubic geometry is inconvenient for doing collective work in dense modular packings. The *stochastic assembly system*[8] is in turn mechanically passive and relies on its ambient fluid medium for reconfiguration. One of the most interesting module designs is the *catom*.[9,10] It is a cylindrical or spherical module without moving parts, which moves by rolling and uses electric or magnetic forces for attachment and actuation. Spherical catoms are well suited for doing collective work in dense, three-dimensional systems, and we shall use them in our investigations.

As regards the problem of reconfiguration planning for dense modular structures, the research has usually been carried out in an abstract way with respect to lattice-based systems.[1,6,11–14] In these

* Corresponding author. E-mail: jleng@ippt.pan.pl

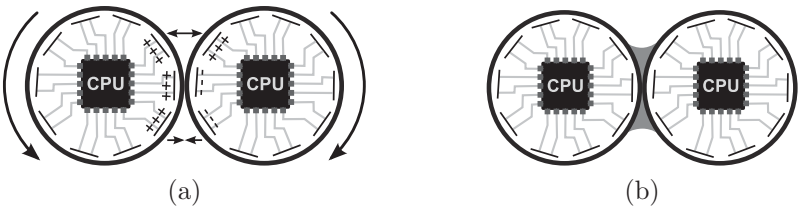

Fig. 1. Active/weak (a) and fixed/strong (b) connections.

works, a complicated reconfiguration problem is solved under purely geometric constraints, like avoiding the overlap of modules and preserving the connectivity of the entire structure, while ignoring by necessity the mechanics of reconfiguration. Conversely, the stiffness of chain-style reconfigurable robots has been also analyzed, but only for already formed configurations.[15] It is, however, crucial whether a planned reconfiguration can be really executed by the actuation mechanisms of modules—in particular, whether the structure will not break or collapse under gravity. We therefore change the usual emphasis and investigate modular structures from the mechanical perspective: use simple reconfiguration scenarios, but analyze stresses and forces more thoroughly.

Our analysis is inspired by the idea of collective actuation.[9] We likewise consider structures made of spherical catoms, in which, however, there is an additional type of connection, strongly binding chosen modules together. An initial analysis of two such structures, serving as linear actuators, has already been presented.[16] Under the assumptions of no friction and a high stiffness of modules, it was shown that the forces produced by these actuators scale with their volumes. However, the inclusion of friction and elastic deformations is necessary to obtain more realistic predictions. In the present work, such more detailed investigations are performed in two ways, analytically and numerically. We analyze one of our previous designs and a new type of structure. Our previous design proves capable of being modified so that its force-volume scalability is preserved in the presence of elastic deformations and friction.

2. Active Microstructures

2.1. Two types of connections

In their original version,[17–20] catoms are held together and actuated by controllable electric or magnetic fields at their contacting surfaces. The resulting forces of attraction bind neighbor modules together, and resulting torques produce rolling motion. Magnetic fields are generated by electromagnets and electric fields by electrodes, placed beneath module surfaces. Electromagnets can potentially produce large forces, but require a constant power supply to maintain them, which is impractical for power-limited systems. By contrast, electrodes only require power for switching, but have rather limited force capabilities.

An electrostatically actuated spherical catom of radius $r = 65\ \mu$m is expected to be able to exert a torque $\tau = 16$ pNm on its neighbor, which allows it to hold, against gravity, six other modules (0.69 μg each) aligned horizontally.[10] The maximum force of cohesion between two such modules is several μN, which is enough to hold about 1000 modules aligned vertically (a 13 cm-high column). A densely-packed arrangement of modules, with four cohesive bonds per module, can be twice as high ($\sim$26 cm), and this is approximately the limit height of any suspended structure. The strength of electrostatic connections cannot be significantly increased, mostly because the voltage between electrodes is limited by air ionization.

Because of the above limitations, we postulate that an additional type of connection is needed between catoms. This new connection type will be called *fixed* or *strong*, and the electrostatic one will be called *active* or *weak* (cf. Fig. 1). Fixed connections are assumed to be much stronger than the active ones, but they are only intended to bind catoms together and need not produce mechanical work or be able to switch on and off very quickly.

Physical realization of fixed connections, capable of being miniaturized, may be difficult, especially if they are required to be simultaneously strong, reversible, energy-efficient and able to form within seconds. The existing large-scale connection mechanisms, like mechanical latches, seem impractical

https://doi.org/10.1017/S026357471500082X Published online by Cambridge University Press

when length scales go down, mainly due to manufacturing problems and extreme precision necessary for docking. Other approaches, suitable for application at the microscale, need to be developed. There exist several physical phenomena which could be used for realizing fixed connections, some of which have already been explored. For example, one can use phase transformations to form reversible soldered connections.[21] However, energy related issues (heating the solder until melting and then its efficient cooling), the time needed to set the connection (several minutes), as well as the relatively small number of reconnection cycles before failure (several hundred), may not result in fixed connections of the required kind. Another possibility might be to use reversible chemical reactions for bonding–debonding,[22] to glue modules together. In that case, it would be necessary to locally control some physical/chemical properties of the environment, which might be difficult to realize in practice. Van der Waals forces, through the use of a "molecular velcro", could also be employed.[23] The problems are obtaining a sufficient strength of the connection and controlling its formation and release, without the need for mechanical breaking. It may turn out that strong electropermanent magnets are the best choice for connections, both active and fixed. Electropermanent magnets only require power for switching, just like electrodes, but their connection strength can be several times greater.[24] The condition is that strong, variable magnetic fields within the system will not disrupt the electronics of the modules.

For the purposes of this study, we shall not further attempt to specify the physics of the fixed connections. We shall only assume that fixed connections of the required kind can be created.

2.2. *Elementary actuation mechanisms*

The two types of connections allow the construction of mechanisms which have a higher structural integrity and can produce much larger forces than structures bound by active connections alone. We call them *active microstructures*. To facilitate further description, we shall also divide the modules forming active microstructures into two types: *active* and *fixed* (by a slight abuse of terminology), depending on the kind of connections they have in the microstructure. Active modules are by definition those which have no strong connections with other modules. They can only have weak connections, and in our analyses they use them to roll over other modules and actuate the microstructures. Fixed modules, on the other hand, have at least one strong connection. In all microstructures discussed in this paper, fixed modules are bound by strong connections into larger groups, further called *fixed structures*, *walls*, *layers* or *frames*. A fixed structure acts as one element and its modules move together for a given period of time. Fixed structures are used to support active microstructures and define their global directions of motion, like animal bones or machine parts. They collect interactions from the active modules, which move between them, and aggregate them into global forces—provided that fixed connections withstand the resulting stresses.

Remark. By convention, modules serving different functions in the microstructure, in particular, modules belonging to different fixed structures, are further denoted by different colors in the figures.

Remark. In general, fixed connections can be formed and released. This has two consequences. First, active modules can become fixed by establishing strong connections, and conversely. Therefore, the division of modules into active and fixed is temporal. Second, fixed structures can evolve by attaching or detaching strongly connected modules. In this paper, however, we do not consider reconfiguration of fixed connections—all fixed connections are established at the beginning and persist through each of the presented analyses. Therefore, active modules remain active and fixed modules remain fixed. Furthermore, fixed structures do not change shape and only move relative to one another. Active modules, on the other hand, reconfigure as discussed in Section 3.3, by rolling over fixed structures and reattaching from one module to the next. In effect, the topology of fixed connections in a microstructure is constant, whereas the topology of active connections changes.

Individual active modules and their immediate neighbors in the microstructure can be arranged in many different ways. The simplest arrangements are those in which there are no weak connections between active modules—only between active and fixed ones—and whose motion is entirely planar. Such local arrangements can be classified into five geometric types, shown in Fig. 2. We call them *elementary actuation mechanisms* or *actuation primitives*.

In the mechanism M-I, an active module rolls over one fixed structure and pushes another fixed structure. In M-II, an active module pushes another active module, which is attached to the same

https://doi.org/10.1017/S026357471500082X Published online by Cambridge University Press

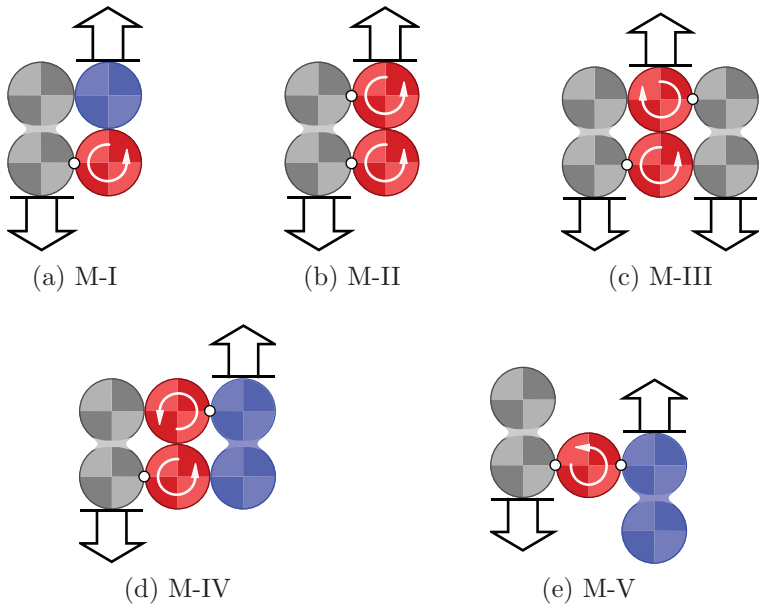

Fig. 2. Elementary actuation mechanisms of active microstructures. Red modules are active—circular arrows indicate their rotation directions. Blue and gray modules are fixed and belong to two different (blue and gray, respectively) fixed structures. White circles between red and blue/gray modules denote active connections, and solid links between two blue or two gray modules denote fixed connections. If neither an active nor a fixed connection is indicated between two contacting modules, then frictional sliding is assumed between their surfaces. Block arrows denote directions of linear motion.

fixed structure and revolves in the same direction. In M-III, an active module pushes another active module, which is attached to the same fixed structure but revolves in the opposite direction. In M-IV, an active module pushes another active module, attached to a different fixed structure. Finally, in M-V, an active module rolls simultaneously, but in opposite directions, over two fixed structures. The mechanisms M-I and M-III are further used to construct two actuator microstructures.

2.3. Examples of linear-actuator microstructures

One can design active microstructures of different shapes, functions and principles of operation. We shall only analyze two microstructures which perform linear motion: the *square linear actuator* and the *pump actuator* with counter-rotating modules.

2.3.1. Square linear actuator. The square linear actuator is one of a family of similar structures which can extend or retract in one direction, as shown in Fig. 3. It is a square column with a cubic arrangement of modules, $2N_x + 1$ modules wide and $N_z + 2$ modules high, built of N_x concentric layers of fixed modules and a line of fixed modules at the center. Two horizontal planes of fixed modules are placed at the top and bottom of the actuator, joining even and odd layers (blue and gray in Fig. 3), respectively, into two fixed frames. There are no weak or strong connections between consecutive layers, whence they can freely slide past each other. In every layer, there is a regular array of *windows*—places where fixed modules are missing. The windows in adjacent layers are "in counterphase," that is they are so arranged that the windows of one layer face a full column of modules of the adjacent layer, and conversely. Every window is filled with an active module (red and yellow in Fig. 3), weakly attached to the modules of the next layer towards the center of the actuator. When they roll, the active modules push the layer, to which they are attached, and the layer, in whose windows they are located, in opposite directions—as shown in Fig. 4. This type of propulsion was classified as the actuation mechanism M-I in Section 2.2. Since the active modules of adjacent layers roll in opposite directions, one frame moves upwards, and the other one downwards, cf. Fig. 3(b).

The principle of operation of the square actuator is analogous to that of a functional subunit of a muscle cell—the sarcomere.[25] A sarcomere is filled with longitudinal filaments of two kinds, made of proteins actin and myosin, respectively, which slide past one another. Heads of the myosin molecules

https://doi.org/10.1017/S026357471500082X Published online by Cambridge University Press

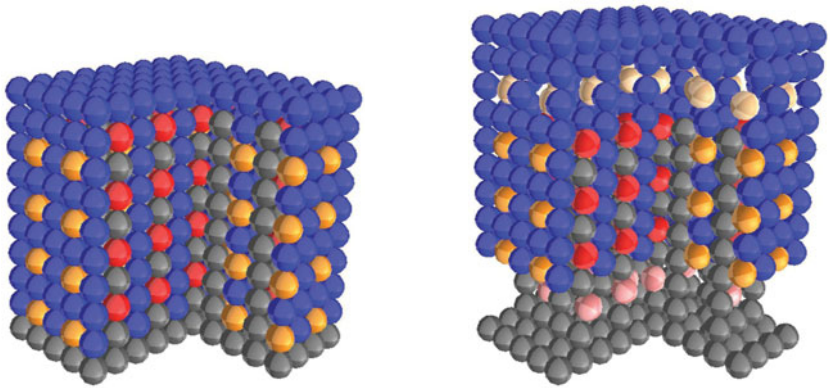

(a) Initial configuration (b) Intermediate configuration

Fig. 3. $N_z \times N_x = 8 \times 4$ single-window square linear actuator, with a front section removed to improve visibility (DEM simulation). Red modules roll downwards and the yellow ones upwards, pushing the gray and blue frames in opposite directions. The modules in pale colors in (b) have deactivated—they stopped pushing the structure. See also Fig. 4.

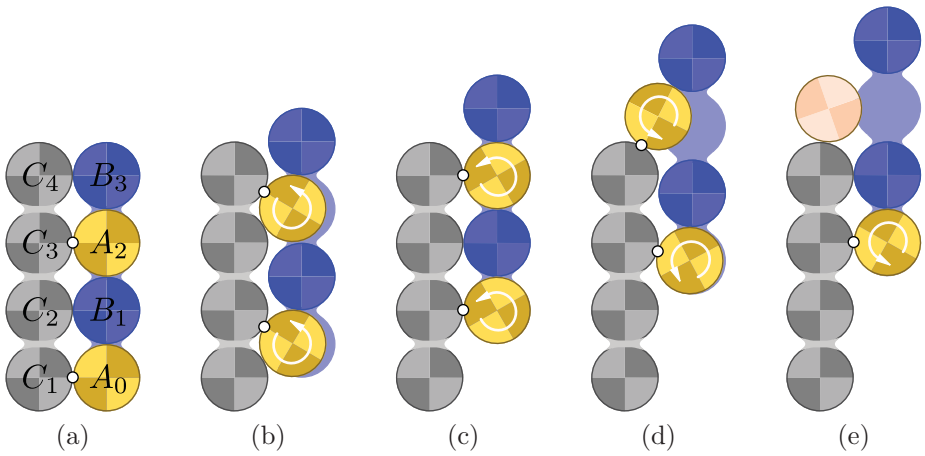

Fig. 4. Five stages of extension of a single-window square linear actuator—cross-section of two layers. The module A_2 in (e) has deactivated—it stopped pushing the structure.

reach out from the myosin filaments, bind to the neighbor actin filaments and pull them, causing contraction of the sarcomere. The produced force is proportional to the volume of the sarcomere, since the heads are distributed along the length of myosin filaments, and the filaments work in parallel. The square actuator is similar—the active modules correspond to the myosin heads, and the layers of fixed modules correspond to the actin and myosin filaments.

Remark. Figures 3 and 4 present a *single-window* square linear actuator, i.e., its windows have dimensions 1×1 modules. In Section 4, we also analyze a *double-window* version, with 1×2 windows, shown in Fig. 14.

2.3.2. Pump actuator with counter-rotating modules. Pump actuators are active microstructures in which active modules are arranged in columns and push one another, as shown in Fig. 5. A pump has counter-rotating active modules if consecutive modules in a column are weakly bound to opposite walls and rotate in opposite directions, as shown in Fig. 6. This arrangement corresponds to the actuation mechanism M-III of Section 2.2. Actuation forces are propagated upwards in a column of N_z active modules, and the top module transfers the resultant force to an upper fixed structure, like the top blue "table" in Fig. 5. The lower part of the pump is a fixed structure (gray modules in Fig. 5) with vertical gaps, into which columns of active modules (yellow and red in Fig. 5) are fitted.

https://doi.org/10.1017/S026357471500082X Published online by Cambridge University Press

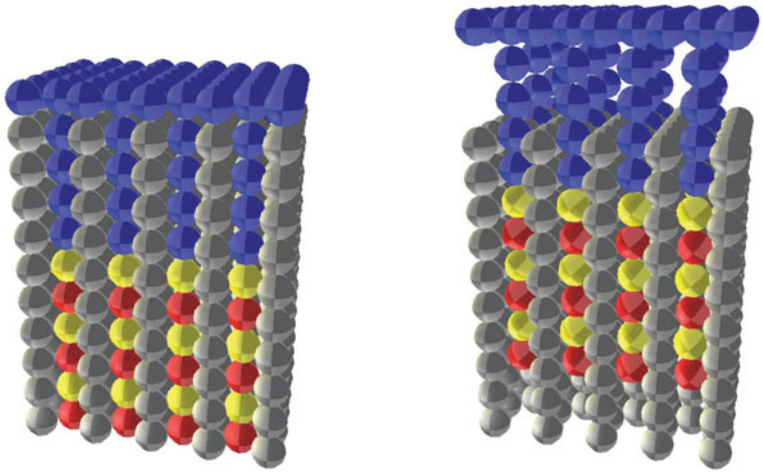

(a) Initial configuration (b) Intermediate configuration

Fig. 5. Pump actuator with counter-rotating modules, having 4×3 columns of active modules (DEM simulation). Red and yellow active modules in each column roll upwards over opposite gray walls, as shown in detail in Fig. 6.

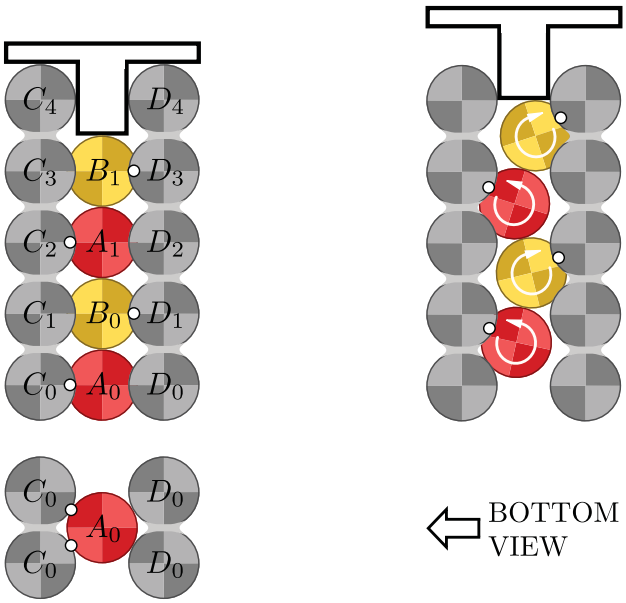

(a) Initial stage (b) Intermediate stage

Fig. 6. One-column pump actuator with counter-rotating modules, capped by a T-shaped external measuring device instead of a piston made of fixed modules. As it is shown in the bottom view, each active module is weakly attached to two fixed modules, to improve the stability of the column.

The operation of the pump actuator is loosely analogous to the flow of a liquid in a pipe, compressed at one end by a piston and open at the other. Fluid pressure builds up towards the piston, just like actuation forces accumulate from the lower to the higher modules in a column, towards the upper fixed structure.

In the rest of the paper, we shall only consider a single column of counter-rotating modules, bounded from above by a horizontal wall or an equivalent measuring device—as shown in Fig. 6. This very simplified setting seems representative of the entire class of structures.

https://doi.org/10.1017/S026357471500082X Published online by Cambridge University Press

3. Modeling and Analysis Methods

3.1. Analytical formulas

Analytical formulas for the overall forces produced by the actuators, as functions of the actuator's extension ΔH, can be derived using the assumptions that the modules are rigid and the motion is quasi-static. Below, they are described in general terms, and the details are provided in the Appendix.

3.1.1. Square linear actuator. The overall force of the square linear actuator is approximately equal to the sum of forces produced by all its active modules, each of which works according to the actuation primitive M-I of Section 2.2. As the actuator extends, its extreme active modules reach the ends of their paths and stop pushing the structure—they *deactivate*, like the module A_2 in Fig. 4(e). In the course of extension, more and more active modules deactivate, until finally none are pushing the structure when it is fully extended.

At any stage of motion, the active modules which have not yet deactivated can be divided into two groups. The first one consists of those active modules, which have not yet reached the level of the last fixed module in the line along which they are rolling. This group includes module A_0 in Fig. 4, and module A_2 in Fig. 4(a)–(b), because they lie lower than the top fixed module C_4. The second group contains those active modules, which have already reached or passed the level of the last fixed module. The module A_2 in Fig. 4(c) enters group 2, and in Fig. 4(d), it deactivates and exits group 2.

The positions of all modules of the same group with respect to their neighbors in the microstructure are the same. Therefore, forces produced by the modules of the same group are also equal, and the overall force of the square linear actuator becomes

$$F_{\mathrm{sq}}(\Delta H) = n_1(\Delta H) f_{\mathrm{I}}(h_1(\Delta H)) + n_2(\Delta H) f_{\mathrm{I}}(h_2(\Delta H)), \tag{1}$$

where $n_1(\Delta H)$ and $n_2(\Delta H)$ are the numbers of modules in groups 1 and 2, respectively, when the actuator is extended by ΔH, $f_{\mathrm{I}}(h)$ is the force produced by a single actuation primitive M-I as a function of its local displacement h (cf. Fig. 21(a)), while $h_1(\Delta H)$ and $h_2(\Delta H)$ are the values of h for groups 1 and 2, respectively, at ΔH. f_{I} is given by Eq. (16) in Appendix A.1 with $k = 1$.

The values of h_1 and h_2 are

$$h_1(\Delta H) = (\Delta H + h_0) \bmod 2r - h_0, \tag{2}$$

$$h_2(\Delta H) = \Delta H \bmod 2r, \tag{3}$$

where r is the module radius, $x \bmod y = x - \lfloor x/y \rfloor y$, $\lfloor \cdot \rfloor$ is the floor function and $h_0 = (3 - \sqrt{4\sqrt{3} - 3})r$ is the vertical distance between the positions of the module B_3 in Figs. 4(b) and (c).

The numbers of modules in groups 1 and 2 are

$$n_1(\Delta H) = n_{\mathrm{x}} \left(\left\lceil \frac{N_{\mathrm{z}} - 1}{p} \right\rceil - \left\lfloor \frac{\Delta H/2r + p - 1}{p} \right\rfloor \right), \tag{4}$$

$$n_2(\Delta H) = n_{\mathrm{x}} \left\lfloor \frac{(\Delta H/2r + p - \sqrt{3}) \bmod p}{p + 1 - \sqrt{3}} \right\rfloor, \tag{5}$$

where $n_{\mathrm{x}} = 2N_{\mathrm{x}}(N_{\mathrm{x}} + 1)$ is the number of active modules which deactivate simultaneously, $\lceil \cdot \rceil$ is the ceiling function and p is the vertical distance, in module diameters, between consecutive active modules: $p = 2$ for the actuator with single windows, and $p = 3$ for the version with double windows.

3.1.2. Pump actuator with counter-rotating modules. In the case of the pump actuator with counter-rotating modules, the computation of the overall force involves a recursive procedure, as opposed to a summation of forces of individual active modules. This is because, in general, the forces transferred from the lower to the higher active modules in the column follow a complex path, and the contributions of individual modules do not directly sum.

https://doi.org/10.1017/S026357471500082X Published online by Cambridge University Press

The vertical force exerted on the measuring device by a single column of N_z active modules, cf. Fig. 6, is

$$F_{\text{pump}}(\Delta H) = f_{\text{III}}(h(\Delta H)), \tag{6}$$

where $f_{\text{III}}(h)$ is computed using the procedure described in Appendix A.2, with $n = N_z$ and $k = \sqrt{3}/2$. ΔH is the vertical displacement of the measuring device from its initial position, and h is the local displacement of the top active module, cf. Fig. 22, given by

$$h(\Delta H) = (\Delta H + r) \bmod 2r - r. \tag{7}$$

If the pump contained many parallel columns of active modules, as in Fig. 5, the total force would be the sum of forces produced by the individual columns.

3.2. Numerical modeling

We simulate active microstructures using Yade,[26] open-source DEM software. Modules are modeled as elastic balls of radius r, Young's modulus E, Poisson's ratio ν and Coulomb friction coefficient μ. There are three structural aspects of active microstructures which are specially handled: strong connections, weak connections and the actuation mechanism of modules.

Strong connections are modeled as cohesion, using a built-in functionality of Yade. The cohesive interaction at a fixed connection constrains all six degrees of freedom. It imposes a normal force, two shear forces, a twisting moment and two bending moments on the point of contact. The elastic stiffness coefficients of the connection are computed from the E, ν and r of the connected modules, using standard formulas of DEM.[27] Two cohesion parameters, one for the normal and one for the tangential direction, determine the strength of the connection in tension and shearing, respectively. A connection breaks if either one of these limiting values is exceeded by the forces acting at the contact point (by default, bending and twisting moments cannot break the connection). As a result, strongly connected modules cannot freely move with respect to each other.

Weak connections are also modeled as cohesion, but with only normal and shear forces at a contact point, and without the bending and twisting moments. This connection, like the strong one, prevents the separation and sliding of modules but, unlike the strong one, allows the modules to freely twist and roll about their contact point. It thus lets active modules move and actuate the microstructure. As in the case of the strong connection, two cohesion parameters determine the strength of the weak connection in tension and shearing.

The actuation mechanism is modeled as a torque applied to an active module. This simple approach is sufficient for making force measurements. The torques acting on all active modules have the same magnitude and are kept constant during each simulation. The directions of the torques are always so chosen as to make active modules roll along selected lines of fixed modules.

Remark. In the simulations, it is assumed that the strength of the microstructures is limited by the torques applied to active modules, and accordingly that both the fixed and the weak connections are able to withstand the stresses. Therefore, the cohesion parameters are set high enough to prevent contact breaking.

3.3. Reconnection control

When an active module rolls along a line of fixed modules, it periodically comes into contact with a new fixed module. At this point, it must break the weak connection with its previous neighbor and establish a weak connection with its new neighbor. Within the modeling scheme described in Section 3.2, this requires that cohesion be established at the new contact point, and be switched off at the old contact point. To facilitate this, a modification was made to the laws of cohesion in Yade. It consisted in assigning three parameters to each module, and establishing conditions for deciding whether contacting modules cohere or not.

The first parameter, *module type*, is an indicator, whether a module is active or fixed.

The second parameter, *material*, is a standard quantity in Yade. Different modules can be defined as made of different materials with identical physical properties. Unlike in the standard code, however, it has been made possible to define the strength of cohesion for each pair of materials independently. In particular, materials which do not cohere are assigned a zero strength of cohesion. Materials are

https://doi.org/10.1017/S026357471500082X Published online by Cambridge University Press

used to define entire groups of modules which can attach to one another, either by fixed or active connections.

The third parameter, *index*, is a positive integer. An active module can attach only to those among its neighbor modules, which have the highest index. By contrast, fixed modules make attachments regardless of indexes—only on the basis of material pairs. Indexes can be assigned in ascending sequences to lines of fixed modules, to let active modules travel along them.

The modified cohesion law can be summarized as follows. Modules are divided into active and fixed. A fixed module can attach to its neighbor, if their materials cohere. An active module can attach to its neighbor, if their materials cohere and if that neighbor has the highest index among all neighbors of the active module. Finally, two adjacent modules establish cohesion, if the first one can attach to the second and conversely—the conditions must be satisfied both ways. The proposed cohesion law allows simple reconnection control, which is only based on local information.

An example assignment of materials and indexes to a fragment of a pump actuator is shown in Fig. 6. Capital letters with subscripts denote materials with indexes. The material pairs that cohere are AC, BD, which correspond to active connections, and CC, DD, which correspond to fixed connections. The modules with materials A and B are marked as active, and those with C and D as fixed. All fixed modules form strong connections with their neighbors of the same material group, regardless of indexes. At the beginning, as shown in Fig. 6(a), A_0 has three neighbors, B_0, C_0 and D_0. Since their highest index is 0, and only the pair AC coheres, a weak connection is formed between A_0 and C_0. Similarly, B_0 has four neighbors, A_0, A_1, C_1 and D_1. Their highest index is 1, and only the pair BD coheres—therefore, a weak connection is formed between B_0 and D_1. At a later stage, shown in Fig. 6(b), A_0 has reattached from C_0 to C_1, since the latter has a higher index. Similarly, B_0 has reattached from D_1 to D_2. A_1 and B_1 behave analogously, as well as the modules of the square linear actuator shown in Fig. 4.

4. Numerical Results

The actuators are placed between upper and lower bounding walls, and are analyzed in terms of the overall force they exert on the walls as they extend (elongate). The force is measured at equilibrium (the so-called quasi-static force) and it does not account for inertia or any other rate-dependent effects. The effects of contact friction and elastic deformations are accounted for in modeling. In all simulations, the values of the module radius and actuation torque are $r = 65\ \mu$m and $\tau = 16$ pNm, respectively. Gravity is neglected.

4.1. DEM force measurement procedures

In the presented simplified DEM model, Newton's laws of motion are directly integrated over time (explicit time integration scheme). During the analysis, the interaction forces are in general not in equilibrium. A special procedure is therefore necessary to capture only the static (equilibrium) forces at a given elongation of an actuator.

The basic version of the procedure consists of three steps that are cyclically repeated until a desired final elongation is attained, cf. Fig. 7. In the first step, A–B, the upper bounding wall is moved a bit upwards in order to allow the actuator to elongate. Next, B–C, the wall stops and the actuator moves against it, until a balance of forces is attained (force oscillations are reduced by the numerical dissipation applied). The third step, C–D, is a short time interval over which the reaction force at the upper wall is sampled and averaged.

The above procedure determines the force that is exerted by the actuator as it elongates. This force is referred to as the *lifting force*. However, as presented in Appendix A.1.2, another situation can be considered, in which the actuator is trying to extend, but it is being compressed by the bounding walls. In this situation, the force applied to the walls is referred to as the *yield force*, and it is greater than or equal to the lifting force. In some cases, the yield force can even be infinite, which means that the structure is wedged by friction.

In order to capture the yield force, the basic procedure is extended by additional three steps, cf. Fig. 7. In step four, D–E, the upper bounding wall is moved downwards in order to compress the structure. Then, in steps five and six, similarly to steps two and three, the wall stops to allow the system to balance the forces, E–F, and the averaged reaction force is then measured, F–G.

https://doi.org/10.1017/S026357471500082X Published online by Cambridge University Press

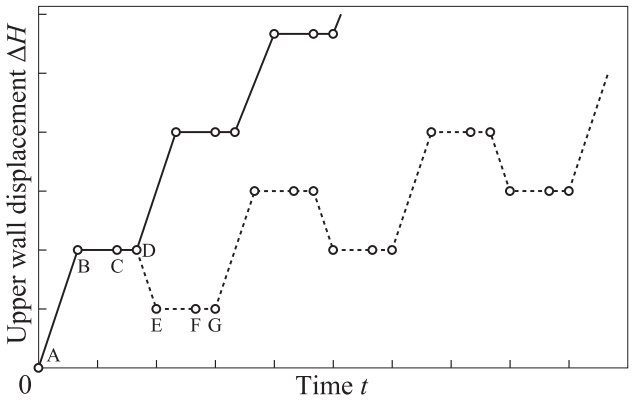

Fig. 7. Loading programs for measuring the overall lifting force (solid), and overall lifting and yield forces (dashed).

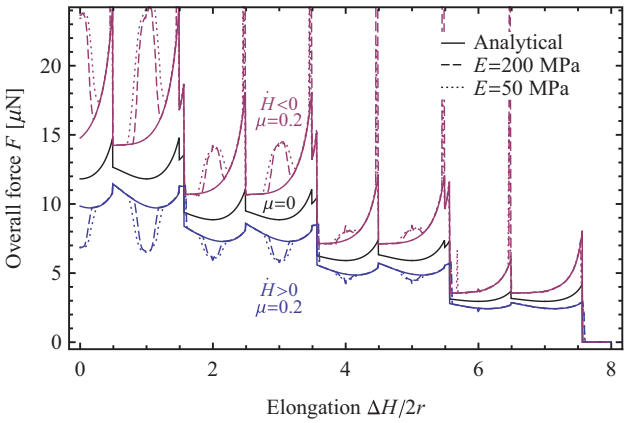

Fig. 8. Force-elongation plot for the 8×2 single-window square linear actuator. The lifting force (blue) and the yield force (purple) for $\mu = 0.2$. The analytical curves (solid) are compared with the numerical solutions for $E = 200$ MPa (dashed) and $E = 50$ MPa (dotted). The reference frictionless overall force (solid, black) is drawn in between. $\dot{H}$ is the elongation velocity.

4.2. Square linear actuator—single-window version

A sample plot of the lifting and yield forces as functions of elongation, for the frictional and frictionless case, is presented in Fig. 8. The decrease of forces in subsequent cycles (every $2r$ of ΔH) is related to the fact that subsequent layers of active modules deactivate, cf. modules in pale colors in Fig. 3(b).

In the frictionless case, the lifting and yield forces are equal and well match the analytical results. In the frictional case, the two forces are different, and there is a significant discrepancy between the numerical and analytical results around ΔH equal to the multiples of $2r$. The region of discrepancy broadens with a decreasing elastic modulus, which indicates elastic deflections of the structure as a possible cause of the observed effect.

The effect of friction on the overall forces is presented in Fig. 9 for two different friction coefficients (only the first two elongation cycles are presented to improve clarity). A deviation from analytical results can be observed at ΔH close to the multiples of $2r$ and it is noticeably higher for larger friction coefficients. A yield force discrepancy is also visible for elongations at which reconnection occurs (r and $3r$), best seen in Fig. 11, and this is an artefact of the simplified reconnection scheme applied, cf. Section 3.3. Namely, once an active module reattaches from one fixed module to another, it cannot reattach backwards. Therefore, when the structure is being compressed during yield force measurements, it gets blocked in the vicinity of reconnection points.

One of the most important properties of active microstructures is how efficiently they transform microactuation into macroscopic work. We quantify it using the measure of mechanical energy

https://doi.org/10.1017/S026357471500082X Published online by Cambridge University Press

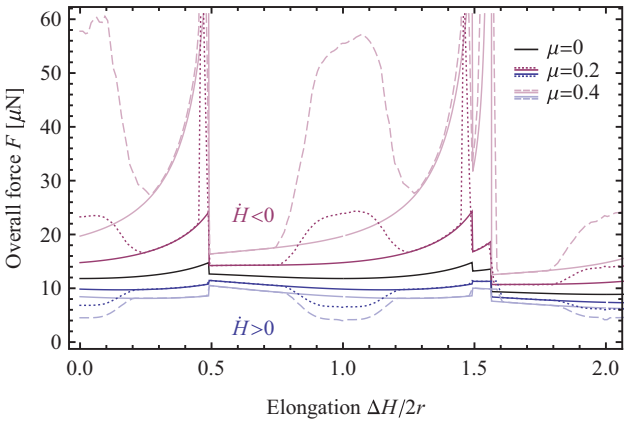

Fig. 9. Force-elongation plot for the 8×2 single-window square linear actuator: the lifting force (blue) and yield force (purple) for $\mu = 0.2$ (dotted, dark) and $\mu = 0.4$ (dashed, pale) are compared with the analytical results (solid lines). The reference frictionless overall force (black) is drawn in between. The dotted and dashed lines are DEM results for $E = 100$ MPa. $\dot{H}$ is the elongation velocity.

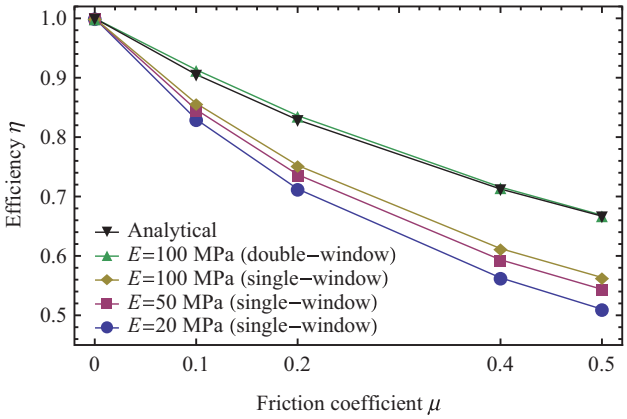

Fig. 10. Decrease of the mechanical energy conversion efficiency η with an increasing friction coefficient, for the 8×2 single-window square linear actuator and different Young's moduli. Analytical results (black triangles) and results for the 12×2 double-window actuator (green triangles) are shown for comparison.

conversion efficiency η,

$$\eta = W_{\text{out}} / W_{\text{in}}, \tag{8}$$

where $W_{\text{in}} = \tau \Delta\varphi$ is the mechanical work of the microactuation of one active module over a cycle, and

$$W_{\text{out}} = \int_0^{\Delta H} \overline{F}(h) \mathrm{d}h \tag{9}$$

is the corresponding mechanical work done by the structure per active module, where $\overline{F} = F/n_{\text{active}}$ is the lifting force per active module. For the square linear actuator, we put $\Delta\varphi = 2\pi/3$ and $\Delta H = 2r$, which are the total revolution of an active module and the total elongation of the actuator, respectively, in the course of one elongation cycle.

Figure 10 shows that η decreases with an increasing friction coefficient and decreasing Young's modulus, which quantifies the tendency observed in Fig. 9. The decrease of η with a decreasing Young's modulus is also presented in Fig. 12(a) (solid lines). The reduction of efficiency is significant; however, it does not seem to be prohibitive for the analyzed Young's modulus range, especially for lower friction coefficients.

https://doi.org/10.1017/S026357471500082X Published online by Cambridge University Press

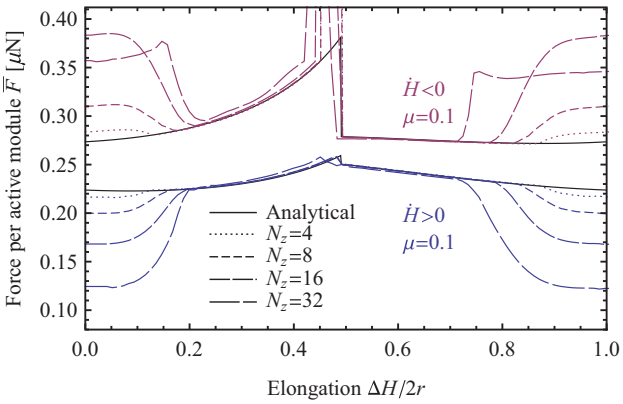

Fig. 11. Lifting and yield forces per active module for a single-window square linear actuator of dimensions $N_z \times N_x$ from 4×1 to 32×1, and $E = 100$ MPa. $\dot{H}$ is the elongation velocity.

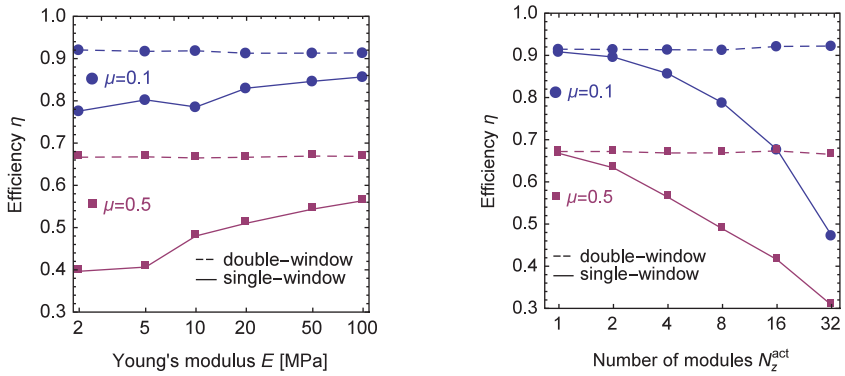

Fig. 12. Comparison of mechanical energy conversion efficiencies of the single-window (solid) and double-window (dashed) square linear actuators for two friction coefficients: $\mu = 0.1$ (blue) and $\mu = 0.5$ (purple). The compared single- and double-window versions have dimensions $2N_z^{act} \times N_x$ and $3N_z^{act} \times N_x$, respectively, so that they have the same width $2N_x + 1$ and the same number N_z^{act} of active modules along their height. The results in (a) are for $N_x = 2$, $N_z^{act} = 4$ and varying elastic stiffness of modules E, and in (b) for $E = 100$ MPa, $N_x = 1$ and varying N_z^{act} (varying height of the actuators).

More disadvantageous is the decrease of the lifting force with an increasing height of the structure, cf. Fig. 11, also expressed in terms of the efficiency parameter η in Fig. 12(b) (solid lines). The energy loss is prohibitively high for higher structures, e.g., the efficiency drops below 50% for the actuator made of 64 modules in the vertical direction and $\mu = 0.1$.

The efficiency drop due to frictional dissipation depends on the normal contact forces, which in the considered case are well reflected by the vertical stresses σ_{zz} in the modules. The values of σ_{zz} in two adjacent walls of an 8×6 actuator are presented in Fig. 13 for the initial ($\Delta H = 0$) and an intermediate ($\Delta H = r$) state. In fixed modules, as expected, σ_{zz} increases in the direction of elongation. In the initial state, Fig. 13(a), the active modules are also subjected to substantial loading, which is an unwanted side-effect of the dense packing of modules. They are compressed between the upper and lower wall modules, as the windows in the walls become shorter due to elastic deformation. Higher contact stresses cause higher frictional dissipation and energy losses. In the intermediate state, Fig. 13(b), the active modules lie out of the plane of the windows, and their σ_{zz} stresses are low.

4.3. Square linear actuator—double-window version

In order to prevent the decrease of the lifting force observed for the single-window square linear actuator, an improved double-window design is proposed, cf. Fig. 14. The idea is a direct consequence of the conclusions from the analysis of the σ_{zz} stresses. The windows in the walls are now twice higher in order to compensate for the compression of the structure. The vertical stresses σ_{zz} in the

https://doi.org/10.1017/S026357471500082X Published online by Cambridge University Press

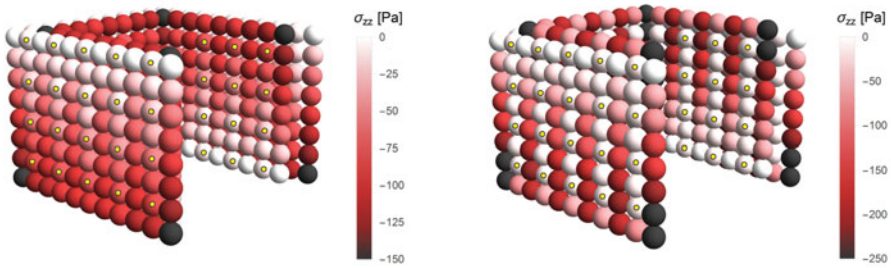

(a) $\Delta H/2r = 0$ (b) $\Delta H/2r = 0.5$

Fig. 13. σ_{zz} for a chosen fragment of the 8×6 single-window square linear actuator. Dots indicate active modules.

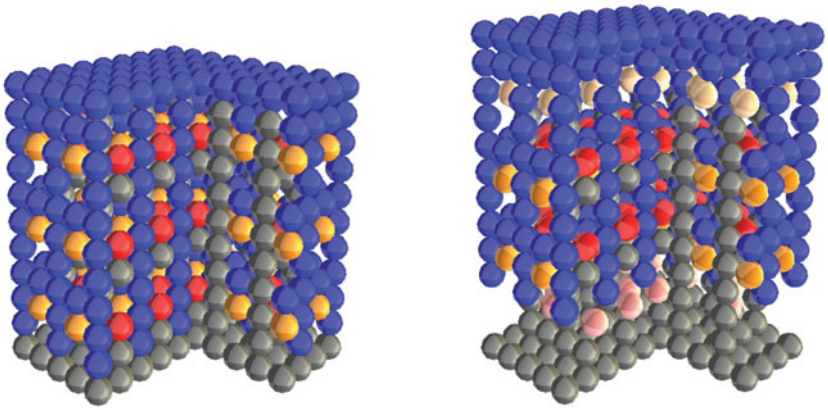

(a) Initial configuration (b) Intermediate configuration

Fig. 14. 9×4 double-window square linear actuator (DEM simulation). The red modules have empty space above them, and the yellow ones have empty space below them, so they can freely fit in the windows.

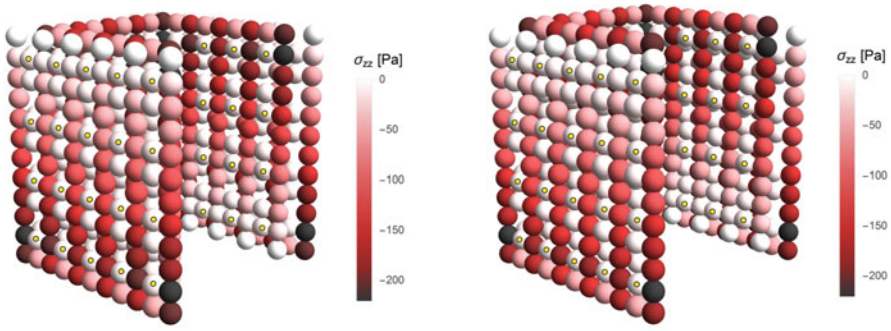

(a) $\Delta H/2r = 0$ (b) $\Delta H/2r = 0.5$

Fig. 15. σ_{zz} for a chosen fragment of the 12×6 double-window square linear actuator. Dots indicate active modules.

double-window actuator, cf. Fig. 15, show that the active modules are now able to freely fit in the windows even at the most demanding elongation phases (when ΔH is equal to the multiples of $2r$).

Figure 16 demonstrates the advantages of the new design, in that the force drops are no longer observed. The numerical results for the double-window version match analytical results very well, and therefore the latter are not shown in Fig. 16. A comparison of the two analyzed designs in terms of their efficiencies is presented in Fig. 12. For the double-window actuator, η is almost independent of both the elastic stiffness, cf. Fig. 12(a), and the height of the actuator, cf. Fig. 12(b). Since η quantifies the contribution of an average active module to the overall work done by the actuator, Fig. 12(b)

https://doi.org/10.1017/S026357471500082X Published online by Cambridge University Press

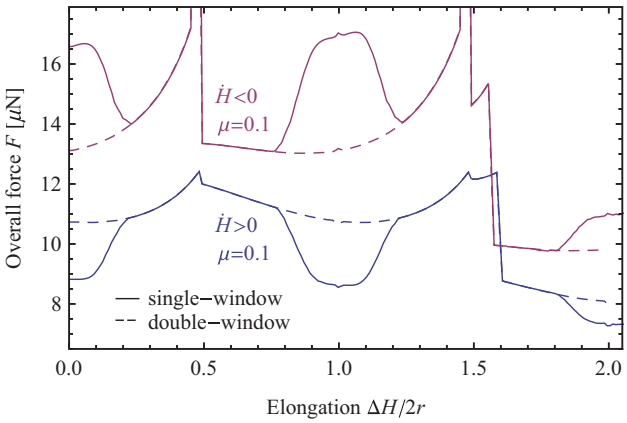

Fig. 16. Comparison of the lifting (blue) and yield (purple) forces of the 8×2 single-window (solid lines) and 12×2 double-window (dashed lines) square linear actuators, for $E = 100$ MPa and $\mu = 0.1$. $\dot{H}$ is the elongation velocity.

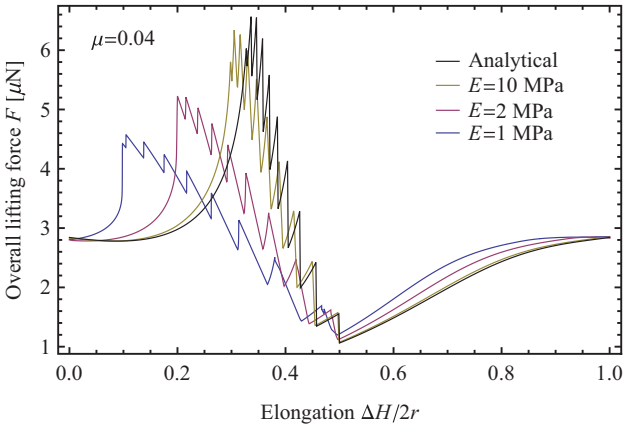

Fig. 17. Lifting force of the $N_z = 10$ pump actuator with $\mu = 0.04$. Comparison of analytical results (black) and numerical results for three different Young's moduli.

implies that the strength of the actuator is proportional to the number of its active modules. And since active modules form a constant fraction of all modules in larger actuators, this finally means that the actuator's strength is proportional to the total number of its modules, and so to its volume. The actuator is therefore scalable.

4.4. Pump actuator

A typical force-elongation plot for one elongation cycle of a pump actuator is presented in Fig. 17. The characteristic sawtooth shape of the graph is caused by a series of subsequent reconnections of active modules when they are climbing the walls. The number of teeth is related to the height of the actuator (number of active modules), as can be observed in Fig. 18.

A significant dependence of the results on the elastic stiffness of modules can be observed, cf. Fig. 17. Nevertheless, the discrepancy between numerical results for elastic modules and analytical predictions for rigid modules has been checked to have a negligible effect on the efficiency η (see Eq. (8) and the definition below) for a wide range of Young's moduli $E = 1$–100 MPa and friction coefficients $\mu = 0$–0.08. For that reason, the efficiency of pump actuators is further examined on the basis of analytical results only.

Force-elongation plots for different actuator heights and different friction coefficients, cf. Fig. 18, show single force peaks per elongation cycle. This is inconvenient for potential practical applications, because it is the lowest, not the highest, lifting force in a cycle that determines the lifting capabilities of an actuator. Moreover, in the case of pump actuators, large output forces cause large frictional

https://doi.org/10.1017/S026357471500082X Published online by Cambridge University Press

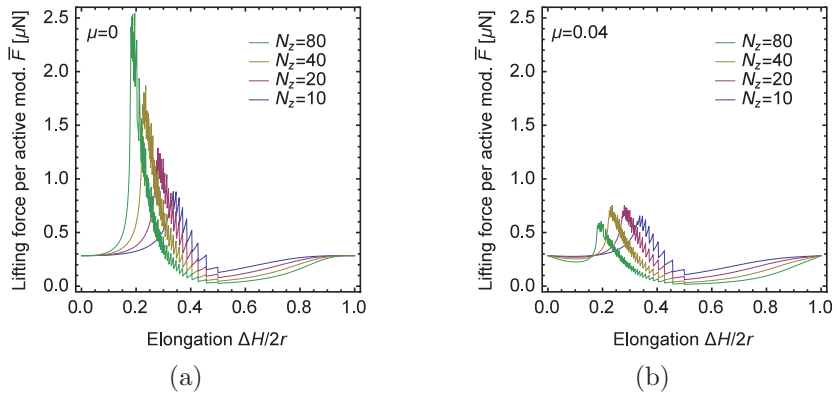

Fig. 18. Analytical lifting force of a pump actuator per active module, for four different actuator heights and (a) $\mu = 0$ and (b) $\mu = 0.04$.

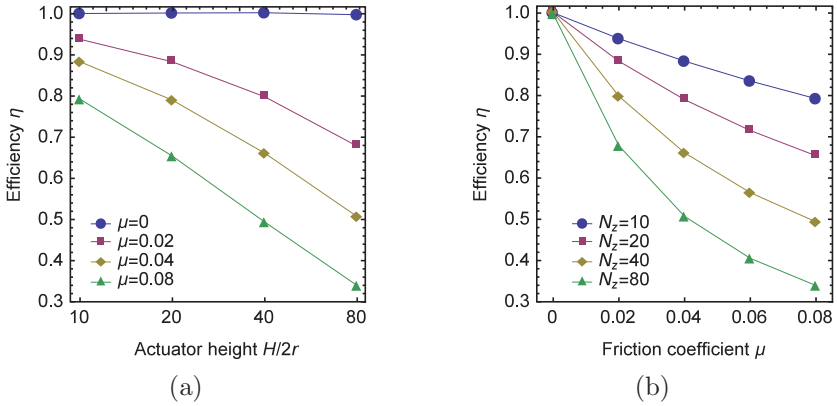

Fig. 19. Analytical energy conversion efficiency of the pump actuator (a) as a function of the actuator's height N_z for four different friction coefficients μ, and (b) as a function of the friction coefficient μ for four different actuator heights N_z.

dissipation. This is clearly visible in Fig. 18, where the force peaks in the frictional case are greatly reduced as compared with the frictionless case, especially for higher actuators.

The influence of friction and the actuator's height can be analyzed in terms of the efficiency η, defined in the same way as in Eq. (8) but with $\Delta\varphi = 4\arcsin(\sqrt{3}/3)$. As can be seen in Fig. 19, even small values of the friction coefficient μ cause a significant decrease of the efficiency of pump actuators. This effect is not entirely intuitive because active modules in the mechanism M-III have compatible directions of rotation. It turns out, however, that the sliding path between neighbor active modules is relatively long, see Appendix A.2.2. This, together with high normal contact forces (forces increase with height, cf. Fig. 20), results in the observed large energy losses.

One can conclude that building tall pump actuators is not practical. However, pump actuators of moderate height can possibly be utilized as building blocks of hybrid pump-linear microstructures.

5. Conclusions and Further Work

We suggested and exploited heterogeneity of inter-module connections, i.e., fixed and strong versus mobile and weak ones. This allowed to improve the strength of modular structures with electrostatic actuation mechanisms, which are fast and practical at the microscale yet too weak to work alone. The fixed connections were assumed to be much stronger, but also more difficult to establish or release, than the active ones. This assumption was incorporated into the proposed designs of modular actuators.

The analysis of the proposed actuators has shown that, when neglecting friction and elastic deformations, the actuators are scalable, i.e., the overall forces they generate are proportional to the

https://doi.org/10.1017/S026357471500082X Published online by Cambridge University Press

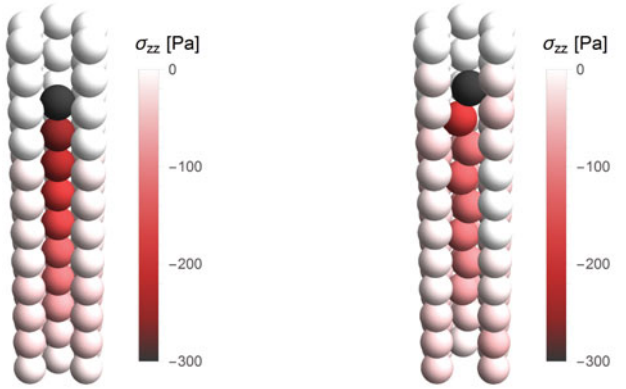

(a) $\Delta H/2r = 0$ (b) $\Delta H/2r = 0.5$

Fig. 20. σ_{zz} stress for a cross-section of an $N_z = 10$ pump actuator at (a) initial and (b) intermediate stage of motion.

number of their constituent modules. This was demonstrated earlier[16] for the single-window square linear actuator and is shown in Fig. 19(a) for the pump actuator. However, in the presence of friction and elastic deformations, a special treatment is necessary to preserve the scalability, and only the proposed double-window version of the square linear actuator proved to be scalable, see Fig. 12(b).

We only analyzed the functionality of actuators whose initial microstructures were already formed. In particular, we investigated reconfiguration of active modules in the simple sense of their motion along predefined straight paths within a structure, and did not discuss reconfiguration of fixed modules at all. The formation of the initial microstructure from other modular arrangements, possibly under load, is a prerequisite for the presented analysis and a very important subject in itself. This topic was not addressed in the present work and requires further investigation.

Acknowledgment

This work was partially supported by the project "Micromechanics of Programmable Matter" (contract no. 2011/03/D/ST8/04089 with the National Science Centre in Poland).

A. Appendix

Below we discuss the vertical forces produced by the actuation mechanisms M-I and M-III. We only consider quasi-static conditions—very slow motion, with no inertia and no gravity. For the sake of generality, all formulas are obtained using an unspecified planar distance $2kr$ between the center of an active module and the fixed modules, to which it is attached. In particular, $k = 1$ for the mechanism M-I used in the square linear actuator, and $k = \sqrt{3}/2$ for the mechanism M-III used in the pump actuator.

A.1. Actuation mechanism M-I

The geometry of the actuation mechanism M-I, cf. Fig. 2, is presented in Fig. 21. We assume that the module B is fixed and that the horizontal distance between B and C is constant and equal to $2kr$. The range of α is $I_\alpha^{\mathrm{I}} = [-\arcsin(1/2k), \arccos(k/(k+1)))$—from the first attachment of A to B to the alignment of B, A and C.

A.1.1. Vertical force f_{I}. The vertical force f_{I}, exerted by A on C, is given by

$$f_{\mathrm{I}} = N \sin\beta + T \cos\beta, \tag{10}$$

where $N \geqslant 0$ is the compressive normal force between A and C, and T is the tangential force. When the structure is moving, T is equal to the force of friction between A and C. Assuming Coulomb

https://doi.org/10.1017/S026357471500082X Published online by Cambridge University Press

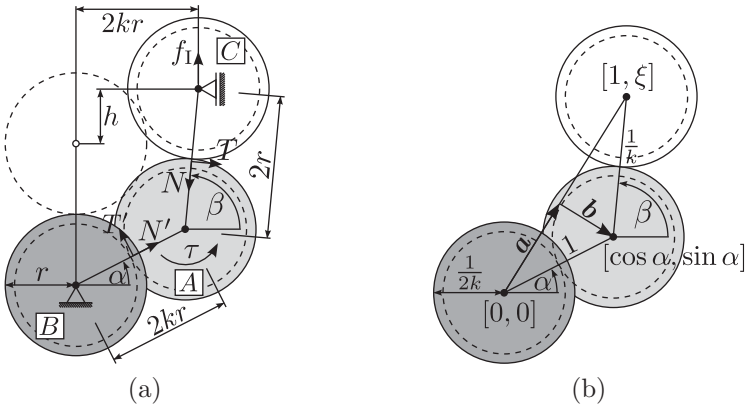

Fig. 21. Mechanism M-I: (a) geometry and forces, and (b) coordinates of the centers of modules and auxiliary variables—with all dimensions divided by $2kr$ and $\xi = (2r + h)/2kr$.

friction, it is given by

$$T = \epsilon \mu N, \tag{11}$$

where $\mu \geqslant 0$ is the friction coefficient, and $\epsilon = \pm 1$ accounts for the direction of sliding between A and C. When A and C move up, the surface of A slides leftwards past the surface of C. The direction of T is then as indicated in Fig. 21, and consequently $\epsilon = 1$. When A and C move downwards, against τ, the situation is reversed and $\epsilon = -1$. Eqs. (10) and (11) together give

$$f_I = N(\sin\beta + \epsilon\mu\cos\beta). \tag{12}$$

The equilibrium of forces acting on A, cf. Fig. 21, reads

$$\begin{bmatrix} N' \\ T' \end{bmatrix} = \begin{bmatrix} \cos(\beta-\alpha) & -\sin(\beta-\alpha) \\ \sin(\beta-\alpha) & \cos(\beta-\alpha) \end{bmatrix} \begin{bmatrix} N \\ T \end{bmatrix}, \tag{13}$$

with the standard trigonometric identities:

$$\begin{bmatrix} \sin(\beta-\alpha) \\ \cos(\beta-\alpha) \end{bmatrix} = \begin{bmatrix} \cos\alpha & -\sin\alpha \\ \sin\alpha & \cos\alpha \end{bmatrix} \begin{bmatrix} \sin\beta \\ \cos\beta \end{bmatrix}. \tag{14}$$

From the equilibrium of torques acting on A, which has the form $\tau = rT + krT'$, and Eqs. (11), (13), one obtains a relation between N and τ:

$$\tau/r = N[\epsilon\mu(1 + k\cos(\beta-\alpha)) + k\sin(\beta-\alpha)]. \tag{15}$$

Finally, by combining Eqs. (12) and (15) to eliminate N, one obtains the required relation between f_I and τ:

$$f_I = \frac{\tau(\sin\beta + \epsilon\mu\cos\beta)/r}{\epsilon\mu(1 + k\cos(\beta-\alpha)) + k\sin(\beta-\alpha)}. \tag{16}$$

The force f_I in Eq. (16) is expressed in terms of the sines and cosines of α and β. They in turn can be expressed as functions of the vertical displacement h, cf. Fig. 21, as

$$\begin{bmatrix} \cos\alpha \\ \sin\alpha \end{bmatrix} = \boldsymbol{a} + \boldsymbol{b} = \frac{a}{x}\begin{bmatrix} 1 \\ \xi \end{bmatrix} + \frac{b}{x}\begin{bmatrix} \xi \\ -1 \end{bmatrix}, \tag{17}$$

$$\begin{bmatrix} \cos\beta \\ \sin\beta \end{bmatrix} = k\begin{bmatrix} 1-\cos\alpha \\ \xi - \sin\alpha \end{bmatrix}, \tag{18}$$

where $\xi = (2r + h)/2kr$, $x = \sqrt{1+\xi^2}$, $a = ||\boldsymbol{a}|| = (x^2 + 1 - k^{-2})/2x$ and $b = ||\boldsymbol{b}|| = \sqrt{1-a^2}$.

https://doi.org/10.1017/S026357471500082X Published online by Cambridge University Press

A.1.2. Lifting force, yield force and wedging. There are two special cases of f_{I}. The first one, f_{I}^{+}, corresponds to the upwards motion of the structure, and is obtained from Eq. (16) by setting $\epsilon = 1$. The second one, f_{I}^{-}, corresponds to the downwards motion (against the torque τ) with $\epsilon = -1$. The former is referred to as the *lifting force* and the latter as the *yield force*, cf. Section 4.1. $f_{\mathrm{I}}^{+} \leq f_{\mathrm{I}}^{-}$, since when the structure is moving upwards, friction acts against τ, and when it is moving downwards, friction acts against f_{I}. The two values coincide when $\mu = 0$.

It can be seen that when $\epsilon = 1$ (the case of the lifting force f_{I}^{+}), Eq. (16) always gives positive and finite values of f_{I} for $\alpha \in I_{\alpha}^{\mathrm{I}}$, and that f_{I} becomes infinite only when B, A and C are aligned ($\alpha = \beta$). On the other hand, when $\epsilon = -1$, there are values of $\alpha \in I_{\alpha}^{\mathrm{I}}$ for which Eq. (16) returns negative values of f_{I}. Since, physically, $f_{\mathrm{I}} > 0$ for $\tau > 0$, therefore at these configurations the system is wedged by friction and in reality $f_{\mathrm{I}}^{-} = \infty$. The intervals of α, in which the system is wedged, can best be determined by analyzing Eq. (12) and Eq. (15) separately, as they give two independent conditions for wedging.

The first condition is obtained from Eq. (12). Since physically, when $\tau > 0$, both $f_{\mathrm{I}} > 0$ and $N > 0$, therefore $\sin\beta - \mu\cos\beta > 0$ must hold when the structure is moving downwards, compressed by f_{I}. Conversely, when $\sin\beta - \mu\cos\beta \leqslant 0$, the structure cannot move. This gives the first condition for wedging:

$$\frac{\sin\beta}{\cos\beta} = \tan\beta \leq \mu. \tag{19}$$

This condition defines two intervals of α, placed symmetrically with respect to $\alpha = 0$, which may or may not intersect with I_{α}^{I}—depending on the value of μ.

The second condition results from Eq. (15). Since $\tau/r > 0$ and $N > 0$, the condition $-\mu(1 + k\cos(\beta - \alpha)) + k\sin(\beta - \alpha) > 0$ must hold when the structure is moving downwards. Conversely, the system is wedged by friction when this condition does not hold, which gives

$$\frac{k\sin(\beta - \alpha)}{1 + k\cos(\beta - \alpha)} \leq \mu. \tag{20}$$

Since the left-hand side of inequality (20), as a function of α, is monotonically decreasing and always has one zero α_0 in I_{α}^{I}, this condition defines one wedging interval of the form $\alpha \geq \alpha_0$.

The system is wedged when either condition (19), or (20), or both, are satisfied. For the usual friction coefficients, satisfying $\mu < 1$, the intervals defined by inequality (19) fall outside I_{α}^{I}. The only wedging interval is $\alpha \geq \alpha_0$ from inequality (20), where α_0 is defined by

$$\frac{k\sin(\beta_0 - \alpha_0)}{1 + k\cos(\beta_0 - \alpha_0)} = \mu, \tag{21}$$

and $\cos\beta_0 = k(1 - \cos\alpha_0)$ by Eq. (18).

A.2. Actuation mechanism M-III

Below we present a procedure for computing the vertical force, f_{III}, exerted by a column of n active modules, A_1 through A_n, working according to the mechanism M-III of Section 2.2, on a bounding wall, perpendicular to the column. The geometry of the mechanism with $n = 3$ active modules is presented in Fig. 22. To shorten the formulas, the following abbreviations are used:

$$\begin{aligned} s_i &= \sin\alpha_i, & c_i &= \cos\alpha_i, \\ \bar{s}_i &= \sin\beta_i, & \bar{c}_i &= \cos\beta_i, \\ s_i' &= \sin(\beta_i - \alpha_i), & c_i' &= \cos(\beta_i - \alpha_i), \\ s_i'' &= \sin(\beta_{i-1} + \alpha_i), & c_i'' &= \cos(\beta_{i-1} + \alpha_i). \end{aligned} \tag{22}$$

The range of α_i is $I_{\alpha}^{\mathrm{III}} = [-\arcsin(1/2k), \arcsin(1/2k))$, which spans the angles between the attachments of A_i to consecutive wall modules.

https://doi.org/10.1017/S026357471500082X Published online by Cambridge University Press

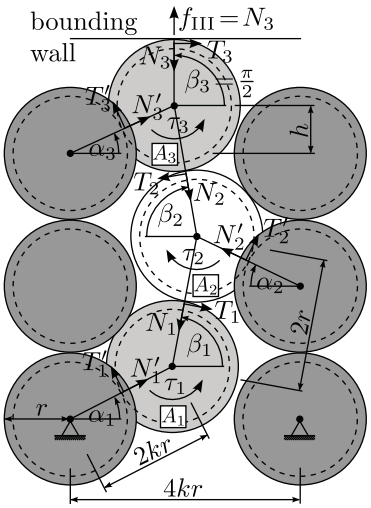

Fig. 22. Geometry and forces of a pump actuator with $n = 3$ counter-rotating active modules, working according to the actuation mechanism M-III.

A.2.1. Vertical force f_{III}. When the structure is moving, the tangential forces between adjacent active modules result from Coulomb friction

$$T_i = \epsilon_i \mu_i N_i, \tag{23}$$

where $\mu_i \geqslant 0$ is the friction coefficient between A_i and A_{i+1}, and $\epsilon_i = \pm 1$ is defined by Eq. (30) and accounts for the direction of sliding between A_i and A_{i+1}, as discussed later.

The equilibrium of forces for the active module A_i, cf. Fig. 22, reads

$$\begin{bmatrix} N'_i \\ T'_i \end{bmatrix} = \begin{bmatrix} c'_i & -s'_i \\ s'_i & c'_i \end{bmatrix} \begin{bmatrix} N_i \\ T_i \end{bmatrix} + \begin{bmatrix} c''_i & s''_i \\ -s''_i & c''_i \end{bmatrix} \begin{bmatrix} N_{i-1} \\ -T_{i-1} \end{bmatrix}, \tag{24}$$

where $N_i \geqslant 0$ is the compressive normal force between A_i and A_{i+1}, and T_i is the corresponding tangential force, whose positive direction is shown in Fig. 22. N'_i and T'_i are the normal and tangential forces, respectively, between A_i and the fixed modules, to which it is attached. From the equilibrium of torques acting on A_i, which has the form $\tau_i - krT'_i - rT_i + rT_{i-1} = 0$, and Eqs. (23), (24), one receives

$$N_i = \frac{\tau_i/r + N_{i-1}[ks''_i + \epsilon_{i-1}\mu_{i-1}(kc''_i + 1)]}{ks'_i + \epsilon_i \mu_i (kc'_i + 1)}. \tag{25}$$

It is a recursive relation, defining N_i in terms of τ_i, N_{i-1} and the respective angles. Since A_1 has no predecessor, therefore $N_0 = 0$ is the initial value for Eq. (25), and since A_n pushes the bounding wall, its normal force equals the overall vertical force exerted by the column

$$f_{\mathrm{III}} = N_n, \tag{26}$$

where N_n is computed by setting $\beta_n = \pi/2$.

The sines and cosines of all angles, cf. Eqs. (22), used in Eq. (25), depend on the vertical displacement $h \in [-r, r)$ of the bounding wall. They are also computed recursively, as is shown below.

It can be inferred from Fig. 22 that $s_n = h/2kr$, $c_n = \sqrt{1 - s_n^2}$. The remaining s_i and c_i are computed recursively downwards, for $i = n - 1, \ldots, 1$. From Fig. 23, one has

$$\begin{bmatrix} c_{i-1} \\ s_{i-1} \end{bmatrix} = \boldsymbol{a} + \boldsymbol{b} = \frac{a}{x} \begin{bmatrix} x_1 \\ x_2 \end{bmatrix} + \frac{b}{x} \begin{bmatrix} x_2 \\ -x_1 \end{bmatrix}, \tag{27}$$

https://doi.org/10.1017/S026357471500082X Published online by Cambridge University Press

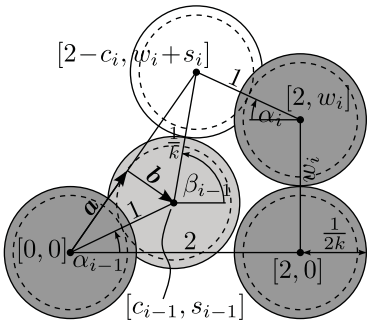

Fig. 23. Coordinates of the centers of modules and auxiliary variables of the actuation mechanism M-III, with all dimensions divided by $2kr$.

where $x_1 = 2 - c_i$, $x_2 = w_i + s_i$, $x = \sqrt{x_1^2 + x_2^2}$, $a = ||\boldsymbol{a}|| = (x^2 + 1 - k^{-2})/2x$, $b = ||\boldsymbol{b}|| = \sqrt{1 - a^2}$ and w_i is a function of s_i discussed below. Since x_1, x_2, a, b and x are functions of s_i and c_i, Eq. (27) defines s_{i-1} and c_{i-1} in terms of s_i and c_i, as required.

The parameter w_i in Eq. (27) may take one of two values. It equals $1/k$ in the situation shown in Fig. 23, when A_i and A_{i-1} are attached to fixed modules which are at different levels. It equals 0 in the case, when A_i and A_{i-1} are attached to fixed modules which are at the same level. The value of w_i can be decided on the basis of s_i:

$$w_i = \begin{cases} 1/k & \text{if } s_i < s_{\min}, \\ 0 & \text{otherwise}, \end{cases} \tag{28}$$

where $s_{\min}$ is a fixed parameter, which depends only on k. In order to determine $s_{\min}$ one can observe that, by definition, $s_i = s_{\min}$ when A_{i-1} is at a reattachment point, i.e., when $w_i = 0$ and $s_{i-1} = -1/2k$. One can now consider a situation symmetric to the one described, in which it is A_i that is located at a reattachment point. In this case, $s_{\min} = -s_{i-1}$ and s_{i-1} can be computed using Eq. (27) by setting $w_i = 0$, $s_i = 1/2k$ and $c_i = \sqrt{1 - s_i^2}$.

Finally, the sines and cosines of β_{i-1} are (Fig. 23)

$$\begin{bmatrix} \bar{s}_{i-1} \\ \bar{c}_{i-1} \end{bmatrix} = k \begin{bmatrix} w_i + s_i - s_{i-1} \\ 2 - c_i - c_{i-1} \end{bmatrix}, \tag{29}$$

and the trigonometric functions of angle combinations are given by the standard expansions:

$$\begin{aligned} s_i' &= \bar{s}_i c_i - \bar{c}_i s_i, & c_i' &= \bar{c}_i c_i + \bar{s}_i s_i, \\ s_i'' &= \bar{s}_{i-1} c_i + \bar{c}_{i-1} s_i, & c_i'' &= \bar{c}_{i-1} c_i - \bar{s}_{i-1} s_i. \end{aligned}$$

Remark. The conditions for wedging of the pump actuator are very complex, because the angles between adjacent modules vary within the column. Nevertheless, one can numerically determine such a value $\bar{\mu}$, which depends on k, that for $\mu_i < \bar{\mu}$, $i = 1, 2, \ldots, n$, there is certainly no wedging regardless of h and the direction of motion of the structure. For $k = \sqrt{3}/2$, as is used in the pump actuator, $\bar{\mu} \simeq 0.316$.

A.2.2. Direction of sliding between modules. The direction of sliding ϵ_i between the adjacent active modules A_i and A_{i+1} changes with α_i, and results in a change of sign of the respective frictional force T_i, cf. Eq. (23). It can be defined as

$$\epsilon_i = \operatorname{sign} v_i, \tag{30}$$

i.e., ϵ_i is the sign of the velocity of sliding between A_i and A_{i+1}. In the upwards motion, by convention, $v_i > 0$ if the surface of A_i slides past A_{i+1} along the direction of motion of A_i, and $v_i \leq 0$ otherwise.

https://doi.org/10.1017/S026357471500082X Published online by Cambridge University Press

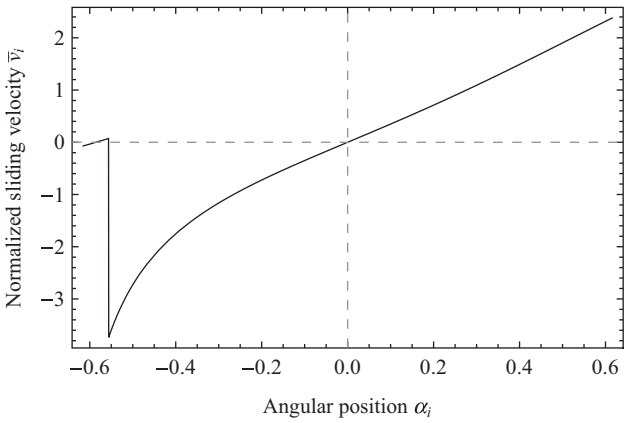

Fig. 24. Normalized sliding velocity $\bar{v}_i$ between the active modules A_i and A_{i+1} in the actuation mechanism M-III over a single cycle, $\alpha_i \in I_\alpha^{\mathrm{III}}$.

In the downwards motion, the sign is reversed. More precisely, v_i can be expressed in terms of the angular velocities as

$$v_i = 2r(\dot{\alpha}_i - \dot{\alpha}_{i+1} - \dot{\beta}_i). \tag{31}$$

By taking the time derivative of Eq. (29), with $i+1$ instead of i, solving the obtained two simultaneous equations for $\dot{\beta}_i$ and $\dot{\alpha}_{i+1}$, and substituting the results into Eq. (31), one receives

$$v_i = 2r\dot{\alpha}_i \frac{s''_{i+1} - s'_i + k\sin(\alpha_i + \alpha_{i+1})}{s''_{i+1}}. \tag{32}$$

As an example, Fig. 24 presents a normalized sliding velocity, $\bar{v}_i(\alpha_i) = v_i/r\dot{\alpha}_i$, for $\alpha_i \in I_\alpha^{\mathrm{III}}$ and $k = \sqrt{3}/2$. This can be further employed to calculate the integral

$$d_{\mathrm{III}} = \frac{1}{2\pi}\int_{I_\alpha^{\mathrm{III}}} |\bar{v}_i(\alpha_i)|\mathrm{d}\alpha_i \simeq 0.23, \tag{33}$$

which is the sliding path length in a single cycle, related to the circumference of the module. The value of 0.23 is lower than in the case of the mechanism M-I ($d_{\mathrm{I}} \simeq 0.33$); however, it is still relatively high and can be a problem for the M-III mechanism. Specifically, due to the build-up of the normal contact forces with height, the total frictional dissipation will be much higher in the pump actuator than in the square linear actuator of corresponding dimensions.

References

1. K. Støy, Emergent Control of Self-Reconfigurable Robots *Ph.D. Thesis* (The Maersk Mc-Kinney Moller Institute for Production Technology, University of Southern Denmark, Odense, Denmark, 2004).
2. M. Yim, Wei-Min Shen, B. Salemi, D. Rus, M. Moll, H. Lipson, E. Klavins and G. S. Chirikjian, "Modular self-reconfigurable robot systems," *IEEE Robot. Autom. Mag.* **14**(1), 43–52 (2007).
3. S. C. Goldstein, J. D. Campbell and T. C. Mowry, "Programmable matter," *IEEE Comput.* **38**(6), 99–101 (2005).
4. S. Murata, H. Kurokawa, E. Yoshida, K. Tomita and S. Kokaji, "A 3-D Self-Reconfigurable Structure," *Proceedings of the IEEE International Conference on Robotics and Automation*, IEEE, Leuven (1998) pp. 432–439.
5. K. Tomita, H. Kurokawa, E. Yoshida, A. Kamimura, S. Murata and S. Kokaji, "Lattice-based modular self-reconfigurable systems," **In**: *Robots and Lattice Automata* (G. Ch. Sirakoulis and A. Adamatzky, eds.) (Springer, 2015).
6. D. Rus and M. Vona, "Crystalline robots: Self-reconfiguration with compressible unit modules," *Auton. Robots* **10**(1), 107–124 (2001).

https://doi.org/10.1017/S026357471500082X Published online by Cambridge University Press

7. J. Romanishin, K. Gilpin and D. Rus, "M-Blocks: Momentum-Driven, Magnetic Modular Robots," *Proceedings of the IEEE/RSJ International Conference on Intelligent Robots and Systems*, IEEE, Tokyo (2013) pp. 4288–4295.
8. M. T. Tolley, M. Kalontarov, J. Neubert, D. Erickson and H. Lipson, "Stochastic modular robotic systems: A study of fluidic assembly strategies," *IEEE Trans. Robot.* **26**(3), 518–530 (2010).
9. J. Campbell and P. Pillai, "Collective actuation," *Int. J. Robot. Res.* **27**(3–4), 299–314 (2008).
10. D. J. Christensen, J. Campbell and K. Støy, "Anatomy-based organization of morphology and control in self-reconfigurable modular robots," *Neural Comput. Appl.* **19**(6), 787–805 (2010).
11. M. De Rosa, S. C. Goldstein, P. Lee, J. Campbell and P. Pillai, "Scalable Shape Sculpting Via Hole Motion: Motion Planning in Lattice-Constrained Modular Robots," *Proceedings of the IEEE International Conference on Robotics and Automation*, IEEE, Orlando, Florida (2006) pp. 1462–1468.
12. P. Bhat, J. Kuffner, S. C. Goldstein and S. Srinivasa, "Hierarchical Motion Planning for Self-Reconfigurable Modular Robots," *Proceedings of the IEEE/RSJ International Conference on Intelligent Robots and Systems*, IEEE, Beijing (2006) pp. 886–891.
13. R. Fitch and Z. Butler, "Million module march: Scalable locomotion for large self-reconfiguring robots," *Int. J. Robot. Res.* **27**(3–4), 331–343 (2008).
14. H. Mabed and J. Bourgeois, "Towards Programmable Material: Flexible Distributed Algorithm for Modular Robots Shape-Shifting," *IEEE/ASME International Conference on Advanced Intelligent Mechatronics (AIM)*, IEEE, Besacon (2014) pp. 408–414.
15. P. J. White, S. Revzen, C. E. Thorne and M. Yim, "A general stiffness model for programmable matter and modular robotic structures," *Robotica* **29**, 103–121 (2011).
16. P. Hołobut, M. Kursa and J. Lengiewicz, "A Class of Microstructures for Scalable Collective Actuation of Programmable Matter," *Proceedings of the IEEE/RSJ International Conference on Intelligent Robots and Systems*, IEEE, Chicago, Illinois (2014) pp. 3919–3925.
17. B. T. Kirby, B. Aksak, J. D. Campbell, J. F. Hoburg, T. C. Mowry, P. Pillai and S. C. Goldstein, "A Modular Robotic System using Magnetic Force Effectors," *Proceedings of the IEEE/RSJ International Conference on Intelligent Robots and Systems*, IEEE, San Diego, California (2007) pp. 2787–2793.
18. J. Reid, V. Vasilyev and R. T. Webster, "Building Micro-Robots: A Path to Sub-mm3 Autonomous Systems," *Nanotech* **3**, 174–177 (2008).
19. M. E. Karagozler, S. C. Goldstein and J. R. Reid, "Stress-Driven MEMS Assembly + Electrostatic Forces = 1 mm Diameter Robot," *Proceedings of the IEEE/RSJ International Conference on Intelligent Robots and Systems*, IEEE, St. Louis, Missouri (2009) pp. 2763–2769.
20. M. E. Karagozler, A. Thaker, S. C. Goldstein and D. S. Ricketts, "Electrostatic Actuation and Control of Micro Robots using a Post-Processed High-Voltage SOI CMOS Chip," *Proceedings of the IEEE International Symposium on Circuits and Systems*, IEEE, Rio de Janeiro (2011) pp. 2509–2512.
21. J. Neubert, A. Rost and H. Lipson, "Self-soldering connectors for modular robots," *IEEE Trans. Robot.* **30**(6), 1344–1357 (2014).
22. W. Dzwolak and P. E. Marszalek, "Zipper-like properties of [poly(l-lysine) + poly(l-glutamic acid)] beta-pleated molecular self-assembly," *Chem. Commun.* **44**, 5557–5559 (2005).
23. D. Thompson, M. Sikora, P. Szymczak and M. Cieplak, "A multi-scale molecular dynamics study of the assembly of micron-size supraparticles from 30 nm alkyl-coated nanoparticles," *Phys. Chem. Chem. Phys.* **15**(21), 8132–8143 (2013).
24. A. N. Knaian, Electropermanent Magnetic Connectors and Actuators: Devices and Their Application in Programmable Matter *Ph.D. Thesis* (MIT, Department of Electrical Engineering and Computer Science, Cambridge, Massachusetts, United States, 2010).
25. R. McNeill Alexander, *Principles of Animal Locomotion* (Princeton University Press, Princeton, New Jersey, United States, 2006).
26. V. Šmilauer, E. Catalano, B. Chareyre, S. Dorofeenko, J. Duriez, A. Gladky, J. Kozicki, C. Modenese, L. Scholtès, L. Sibille, J. Stránský and K. Thoeni, "Yade Reference Documentation," **In**: *Yade Documentation* (V. Šmilauer, ed.) (The Yade Project, 1st ed., online), http://yade-dem.org. 2010.
27. V. Šmilauer and B. Chareyre, "Yade DEM Formulation," **In**: *Yade Documentation* (V. Šmilauer, ed.) (The Yade Project, 1st ed., online), http://yade-dem.org/doc/formulation.html," 2010.